Capillarity

Vol. 11, No. 2, p. 31-40, 2024

Original article

Theoretical and experimental analysis of surface anchoring in the surface stabilization of ferroelectric liquid crystal cells

Rihab Zgueb, Hassen Dhaouadi*

Laboratory of Soft Matter Physics and Fluid Physics (LP2MPF), Faculty of Sciences of Tunis, Université Tunis El-Manar, Campus Universitaire Farhat Hached, Tunis 2092, Tunisia

Keywords:
Chiral smectic liquid crystals
phase transition
electro-optics
surface anchoring energy

Cited as:
Zgueb, R., Dhaouadi, H. Theoretical and experimental analysis of surface anchoring in the surface stabilization of ferroelectric liquid crystal cells. Capillarity, 2024, 11(2): 31-40.
https://doi.org/10.46690/capi.2024.05.01

Abstract:
Based on the response of a chiral smectic liquid crystal to electrical excitation, this paper develops a theoretical calculation to explain the observed phenomenon in a confined structure, with the aim to establish a connection between these phenomena and the surface anchoring energy. To demonstrate the influence of surface anchoring on the observed phase behaviors in the surface stabilization of ferroelectric liquid crystal cells, an experimental validation of the theoretical calculations is conducted. Importantly, it is possible to express the transition thermal shift as a function of the anchoring energy by calculating this energy as a function of the square of the tilt angle. Our calculations allow for the utilization of experimental outcomes in determining distinctive parameters such as the anchoring energy and the elastic constant, two quantities that are essential for understanding and controlling ferroelectric liquid crystal devices.

1. Introduction

The study of phase behaviors in confined configurations is vital in systems that incorporate liquid crystals. For example, for some applications, it is important to know the shift at transitions to determine the optimal operating range of displays or to ensure an acceptable accuracy of temperature indicators based on liquid crystals. Many significant phenomena have been observed in experiments involving chiral smectic liquid crystals. Also, several types of hysteresis are reported in the literature. A delay in transitions under an electric field has been observed in certain phases (Dupont et al., 1988; Roy et al., 1998). Bistability was detected in electro-optic experiments (Yamada and Takanishi, 1997; Sasaki et al., 2012; Chemingui et al., 2016). Ferroelectric hysteresis characterized by non-zero polarization was indicated even in the absence of an exciting field (Dhaouadi et al., 2016). Thermal hysteresis and coexistence phenomena often accompany phase transitions in chiral smectics (Zgueb et al., 2014, 2018).

The anomalies accompanying phase transitions are mainly associated with the confinement imposed by the treated surfaces of surface stabilization of ferroelectric liquid crystal (SSFLC) cells (Riahi et al., 2017; Cai et al., 2023). It was further experimentally demonstrated that cell thickness greatly influences the transition temperature, and even the measured values of the polarization of studied samples are affected (Vaupotic and Copic, 2003; Khan et al., 2021).

Although surface anchoring exerts some undesirable effects, it can be of great value in several applications, such as high-speed, low-power consumption, high-resolution, and high-contrast ratio displays (Srivastava et al., 2015; Guo et al., 2019). Another example of the application of surface effects was proposed by Liu et al. (2022), wherein capillary force can cause the pull-in instability, adhesion between parts, and even failure of the micro/nano functional device.

Theoretical studies on the above phenomena are abundant in the literature, with some relevant ones providing the basis

Yandy Scientific Press

*Corresponding author.
E-mail address: rihab zgueb@yahoo.frm (R. Zgueb); hassen.dhaouadi@ipeit.rnu.tn (H. Dhaouadi).

Received November 15, 2023; revised December 10, 2023; accepted January 10, 2024; available online January 17, 2024.

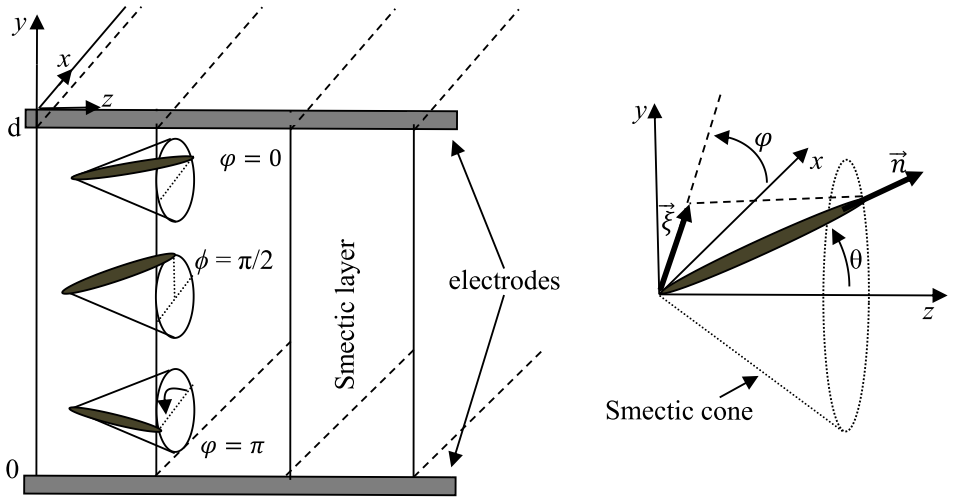

Fig. 1. Variation in the azimuthal angle in sample thickness. Tilt angle $\theta = (\widehat{\vec{n},\vec{z}})$; Azimuthal angle $\varphi = \left(\widehat{\vec{x},\vec{\xi}}\right)$, where $\vec{\xi}$ is the projection of director $\vec{n}$ on the plane (X,Y).

of our research. Roy et al. (1998) described the development of the Landau free energy in the vicinity of the transition from the ferroelectric phase (SmC*) to the smectic A phase and showed that the linear and quadratic coupling between tilt and polarization order parameters is responsible for the increase in the transition temperature T_C with the increase in cell thickness.

Theoretical studies on the response of a chiral smectic liquid crystal to electrical excitation have been abundant (Clark and Lagerwall, 1980; Lagerwall and Dahl, 1984; Biswas and Mukherjee, 2019), which are utilized in this study for the development of a theoretical calculation method. This work aims to express the surface anchoring energies W_s of molecules as a function of the threshold field E_c, the magnitude of the applied electric field from which the liquid crystal molecules lift off from the surface. Computing shows that this energy can be written as a function of the square of the tilt angle, which makes it possible to express the thermal shift of the phase transition as a linear function of temperature W_s.

The first part of this paper presents the theoretical calculation of the free energy of the studied system, taking into account the anchoring energy W_s. The second part includes the presentation of the experimental observations that inspired this study. Finally, the results are discussed and the data of some interesting orders of magnitude are proposed.

2. Theoretical model

2.1 Theory of surface anchoring

Consider a perfect sample of liquid crystal in the mesophase with oriented plane geometry (bookshelf geometry) (Yamada and Takanishi, 1997; Sasaki et al., 2012). The axes of the coordinate system are defined as shown in Fig. 1, where the (Oy) axis is perpendicular to the electrodes and the (Oz) axis is perpendicular to the smectic layers. To simplify the calculations, the following assumptions can be made:

- Incompressible smectic layers (the tilt angle θ remains constant).
- Isotropy of elastic constants.
- Absence of flexoelectricity and dielectric coupling.
- The frequencies used for electro-optical observations are lower than the characteristic frequencies of the system (10 kHz). Thus, the equilibrium can be considered as established at each moment.

2.2 Free energy and characteristic lengths

Firstly, we review the basic calculations that describe the action of an electric field on the chiral smectic sample described previously. The free energy of the system F is written as (De Gennes and Prost, 1993; Khan et al., 2020):

$$F = \iiint_V \left[\frac{1}{2}K(\vec{\nabla}\varphi)^2 - PE\cos\varphi\right] \mathrm{d}V + \frac{1}{2}\iint W_s[\sin^2\varphi_{(y=0)} + \sin^2\varphi_{(y=d)}]\mathrm{d}S \quad (1)$$

where K represents the elastic constant, E represents the applied electric field, P represents the spontaneous polarization, d represents the cell thickness, φ represents the azimuthal angle at the y coordinate, $\vec{\nabla}\varphi$ represents the gradient operator, S represents the active surface of the cell, and V is its volume $(V = Sd)$.

The first item in the above summation is the volume energy containing the electrical and elastic coupling. The second part containing W_s is a surface term corresponding to the anchoring energy of molecules to surfaces. In the absence of any other term, this anchoring energy is minimal for the values of the azimuthal angle $\varphi = 0$ and $\varphi = \pi$. These two values of φ correspond to the two existing states in the planar geometry used (Clark and Lagerwall, 1980). Without an applied electric field, this geometry is compatible with zero spontaneous polarization of the sample. On average, molecular dipoles are oriented in two opposite directions on both sides of the cell.

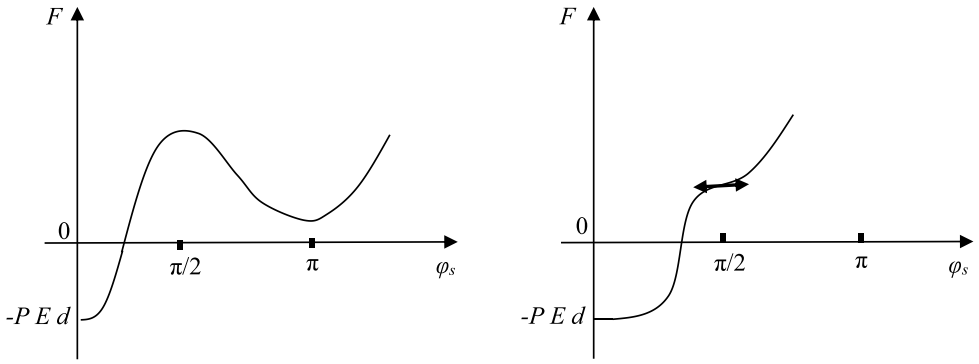

Fig. 2. Free energy as a function of φ_s. (a) For $E < E_c$, there are two minimum values. The chevron structure is retained with $\varphi_s = 0$ or π at the surfaces and (b) for $E > E_c$, the second minimum disappears and the director follows the direction of the applied electric field at both surfaces.

By considering variations only along the "y" direction, the variation in free energy δF can be written as:

$$\delta F = \iiint_V \left\{ \frac{K}{2}\left[\frac{\partial(\varphi+\delta\varphi)}{\partial y}\right]^2 - \frac{K}{2}\left(\frac{\partial\varphi}{\partial y}\right)^2 + PE\sin\varphi\delta\varphi \right\} dV + \iint_S \{W_s[\sin\varphi\cos\varphi_{(y=d)}] + [\sin\varphi\cos\varphi]_{(y=0)}\delta\varphi\} dS \quad (2)$$

After integration and assuming that the problem is one-dimensional, the Euler-Lagrange equation corresponding to Eq. (1) can be expressed as (Appendix):

$$K\frac{\partial^2\varphi}{\partial y^2} - PE\sin\varphi = 0 \quad \text{or} \quad \xi^2\frac{\partial^2\varphi}{\partial y^2} - \sin\varphi = 0 \quad (3)$$

where $\xi^2 = K/(PE)$.

Likewise, from Eq. (3), the surface conditions can be expressed as (Appendix):

$$\begin{cases} K\dfrac{\partial\varphi}{\partial y} + W_s\sin\varphi\cos\varphi = 0 \text{ for } y = d \\ -K\dfrac{\partial\varphi}{\partial y} + W_s\sin\varphi\cos\varphi = 0 \text{ for } y = 0 \end{cases} \quad (4)$$

Notably, $\lambda = K/W_s$ and ξ represent the two characteristic lengths of the problem. The latter appears as the thickness of a thin layer in which the molecules follow the orientation imposed by surface anchoring in the presence of the applied field. When $\lambda \sim \xi$, the anchoring of molecules to the surface is predicted to disappear. The order of magnitude of length ξ can be calculated by taking $K = 5\times10^{-15}$ dyne; P = 10 C/cm^2 and E = 3×10^4 V/cm where ξ = 4 × 10^{-6} cm $\ll d$.

2.3 Analytical resolution

Based on the previous estimates, the surfaces can be separated. This work treats each of them separately and considers a semi-infinite medium. Under these conditions, a prime integral of Eq. (3) can be written as:

$$\frac{\xi^2}{2}\left(\frac{\partial\varphi}{\partial y}\right)^2 + \cos\varphi = \pm 1 \quad (5)$$

The + (respectively -) sign of the second member of Eq. (5) corresponds to the case where $\varphi = 0$ (respectively $\varphi = \pi$) away from the surfaces. In fact, following the application of the electric field in the "y" direction, the molecular dipoles tend to orient themselves in this direction, which gives a director orientation characterized by a constant azimuthal angle. Then, $\partial\varphi/\partial y = 0$, which gives $\cos\varphi = \pm1$ with φ = 0 or $\varphi = \pi$ in volume (Kumar et al., 2019).

By choosing the surface at $y = 0$ and the positive sign of Eq. (5), with $\varphi_{(y=0)} = \varphi_s$, this work obtains:

$$\cos\frac{\varphi_s}{2}\left(2\cos^2\frac{\varphi_s}{2} - 1\right) + \frac{\lambda}{\xi} = 0 \quad (6)$$

This is a cubic equation that can be written in the following form:

$$x^3 - \frac{x}{2} + \frac{\lambda}{2\xi} = 0 \quad (7)$$

where $x = \cos(\varphi_s/2)$.

Solving the above equation yields

- For $-4 + 54(\lambda/\xi)^2 > 0 \rightarrow \left[E \text{ weak}; E < 2W_s^2/(27KP)\right]$, Eq. (7) has three real roots. The two positive roots correspond to $x < 1$; which requires angles φ_s to be between 0 and π. In this case, the free energy function of φ_s has two minima, as seen in Fig. 2(a). The characteristic length ξ is large in a way that although the molecules in the volume follow the orientation imposed by the field (φ = π), the molecules on the surface remain in the potential well corresponding to the initial orientation (φ = 0).
- For $-4 + 54(\lambda/\xi)^2 > 0 \rightarrow \left[E \text{ strong}; E > 2W_s^2/(27KP)\right]$, the free energy has a single minimum as shown in Fig. 2(b) for $\varphi_s = 0$ with $F_s(\varphi_s = 0) = -PEd$, where d represents the cell thickness. The anchoring of molecules on the surface disappears only for a threshold field E_c, defined by:

$$E_c = \frac{2}{27}\frac{W_s^2}{KP} \quad (8)$$

From Eq. (8), the anchoring energy W_s can be determined if the value of the threshold electric field E_c is known. Also,

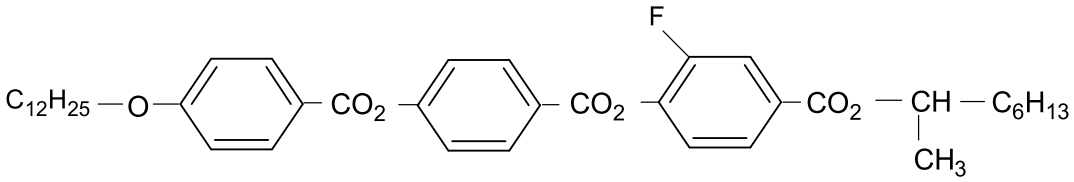

Fig. 3. Structural formula of the compound C12F3.

$-4+54(\lambda/\xi)^2=0$ leads to the following relation between the two characteristic lengths ξ and λ:

$$\lambda=\frac{\sqrt{2}}{3\sqrt{3}}\xi \tag{9}$$

2.4 Threshold field and anchoring energy

In order to measure the anchoring energy, it is necessary to break the anchoring by increasing the amplitude of applied electric field. The removal of molecules from the surface leads to an increase in polarization, which can be assessed through electro-optical measurements. The obtained electro-optical curves have two peaks, as seen later in the "Experimental validation section. The main peak corresponds to the tilting of molecules in the volume; however, the second smaller peak corresponds to the lift off of the molecules from the surface.

The area of the first peak gives the polarization charge in volume $Q=2PS$; however, that of the second peak gives the residual polarization at the surfaces, which corresponds to an electric surface charge Q_s of the following form:

$$Q_s=\frac{4P\xi}{d}S \tag{10}$$

Thus, the ratio of the areas of the two peaks provides a direct measure of the coherence length ξ:

$$\frac{4}{d}\frac{\xi}{}=2\frac{Q_s}{Q} \tag{11}$$

From the values of length ξ, spontaneous polarization P and applied field E, the elastic constant K can be calculated by $\xi=\sqrt{K/PE}$.

The threshold electric field E_c gives the value of the anchoring energy W_s of the molecules on the surface (Eq. (8)). As shown by the experimental curves of variation in the tilt angle θ and E_c, the proportionality between θ and E_c can be established.

It is found in the literature that the elastic constant K is proportional to θ^2. Since spontaneous polarization is also proportional to θ, it follows that the anchoring energy at the surface W_s is proportional to θ^2:

$$W_s=W_0\theta^2 \tag{12}$$

where W_0 represents the constant of proportionality between W_s and θ^2.

2.5 Thermal shift

In order to explain the thermal shift observed at the $SmA\rightarrow SmC^*$ transition, this work considers the Landau-De Gennes development of free energy as a power series of the two parameters of tilt and polarization. Here, only the dominant terms are kept. Then, we add the surface energy term (referred to the unit of volume) $W_s/d=W_0\theta^2/d$:

$$f=f_0+\frac{1}{2}a\theta^2+\frac{1}{2}\frac{1}{\varepsilon_0\chi_\perp}P^2-cP\theta+\frac{W_0}{d}\theta^2 \tag{13}$$

where f_0 represents the free energy in the smectic A phase with θ = 0, ε_0 and $\chi_\perp$ respectively represent the permittivity of vacuum and the susceptibility of the sample, and "c" is the coupling constant between P and θ. In mean-field theory, the coefficient "a" is proportional to $(T-T_c)$ with a constant proportionality coefficient $\alpha: a=\alpha(T-T_c)$.

By minimization, this gives the non-zero values of P and θ in the SmC*phase for temperatures $T<T_c$. The coefficient of the quadratic term of Eq. (13) can be written as:

$$\alpha(T-T_c)+\frac{2W_0}{d}=\alpha\left[T-\left(T_c-\frac{2W_0}{\alpha d}\right)\right] \tag{14}$$

The transition takes place at temperature $T_c^*=[T_c-2W_0/(\alpha d)]$, which corresponds to a shift in transition temperature:

$$T_c^*-T_c=-\frac{2W_0}{\alpha d} \tag{15}$$

The greater the thickness of the cell, the smaller the shift, which will be described later in the experimental part.

3. Experimental validation

Experimental validations of the previous theoretical results were carried out on the compound C12F3. It is a reference product used by members of our liquid crystal research team (Essid et al., 2004; Manai, 2006). The structural formula of the compound C12F3 is given in Fig. 3.

The phase sequence of the studied compound is as follows:

$$Cr\,(60^\circ)-SmC_A^*\,(67.2^\circ\mathrm{C})-SmC_{Fi1}^*+SmC^*\,(79.4^\circ\mathrm{C})$$
$$-SmC^*\,(88^\circ\mathrm{C})-SmC_\alpha^*\,(88.6^\circ\mathrm{C})-SmA\,(106^\circ\mathrm{C})-I$$

Commercial planar cells (3, 5 and 8 μm thicknesses) coated with a conductive layer of indium tin oxide ITO were used for all measurements. The microscopic observation of textures was carried out using a polarizing microscope. Cells of 3, 5 and 8 μm were used for dielectric measurements. For the electro-optical experiments, only the cell with 5 μm was used. A programmable oven ensured temperature control within 0.1 °C.

3.1 Microscopic observation

The theoretical study proposed in Section 2 is based on the assumption of the formation of a chevron structure in

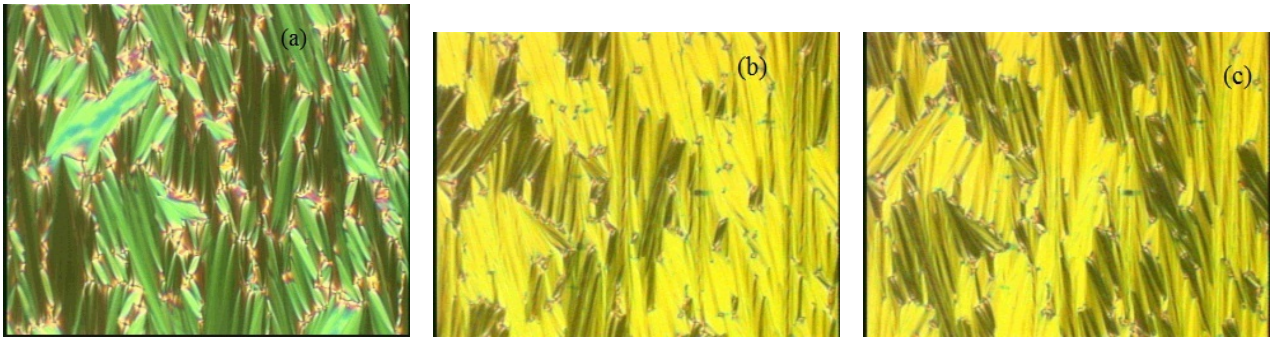

Fig. 4. Photomicrographs obtained by polarized transmission microscopy in 5 μm thick SSFLC cell. (a) SmA phase (T = 90 °C) with specific focal conic defect, (b) SmC* phase at T = 84 °C, and (c) SmC* phase at T = 82 °C, respectively. Note that these geometrical zigzag defects are specific to chevron structure (b) and (c).

the sample. This chevron structure in the SmC* phase is the result of the boundary conditions at the cell surfaces. Specific defects, characterized by a zigzag formation, are generated (Clark and Rieker, 1989). X-ray diffraction is a method that provides tangible evidence of the formation of the chevron structure (Watson et al., 2002). Due to the impossibility of performing X-ray diffraction in this case, this work presents in this section a microscopic observation of the specific defects on a chiral smectic sample exhibiting the SmC* phase confined in a 5 μm thick cell (Fig. 4).

3.2 Thermal hysteresis

The assembly and operating mode used for dielectric and electro-optical measurements are described in detail by Zgueb et al. (2014). The system comprises the following components:

- A programmable function generator (Tektronix AWG2021).
- A high stability amplifier (Krohn-Hite Model 7,500 amplifier).
- A programmable oscilloscope (Agilent 54,622).
- A 7,280 DSP lock-in amplifier.

In the alternating regime, the dielectric permittivity is complex. An often (but not always) used convention is to note ε' as its real part and ε'' as its imaginary part, introduced by a negative sign (-) ($\varepsilon^*(\omega) = \varepsilon' - i\varepsilon''$). The imaginary part of permittivity expresses energy dissipation. In the case of flat surface capacity, this results in a positive real part of the impedance. The measured AC voltage was approximately 0.5 V, and the frequency ranged from 10 to 300 kHz. The frequency-dependent complex permittivity of the liquid crystal was analytically described by the generalized Cole–Cole model (Cole and Cole, 1941).

Fig. 5 shows the temperature dependence of the real part of dielectric permittivity of the sample for the studied cells with thicknesses of 3, 5 and 8 μm. The first small jump indicates the transition from the SmA phase to the SmC^*_α one, and the second larger jump corresponds to the SmC^*_α-SmC* transitions. The feature of interest in this figure is the shift in transitions: the transition to the ferroelectric phase occurs in the 3 μm thick cell at higher temperatures compared to those observed for the other two thicknesses (around 3-4 °C). This

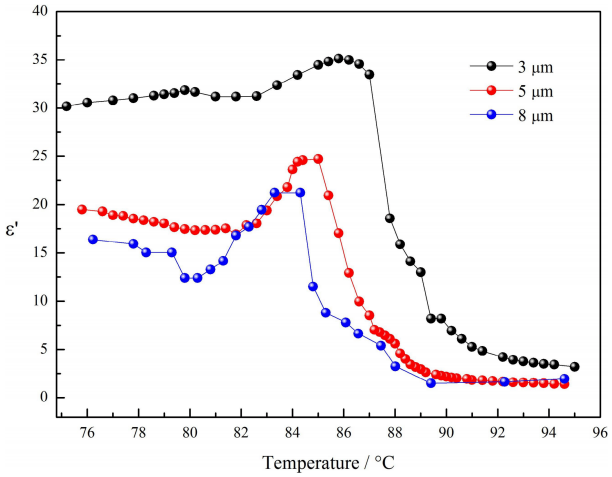

Fig. 5. Dependence of ε' for 3, 5 and 8 μm cell thickness with temperature. Measurements were carried out during the cooling process, with a frequency f = 200 Hz.

observation suggests a connection between this shift and the anchoring force on the surface. Another interesting feature is the variation in dielectric permittivity with the cell thickness. In an SSFLC cell, the surface anchoring blocks the Goldstone fluctuation mode on a boundary layer whose thickness depends on the strength of anchoring; therefore, only the volume molecules contribute to the dielectric response of the sample. This can explain the fact that the dielectric permittivity diminishes with the decreasing thickness of the cell. In fact, for low thickness, the Goldstone mode is also blocked in volume.

Among the parameters needed in the following discussions are the spontaneous polarization P of the sample and the tilt angle θ. These two parameters have occasionally been measured by the electro-optical method on the 5 μm thick cell during the cooling process. The results are shown in Figs. 6 and 7. The temperature dependence of P and θ faithfully follows Landau's first law.

3.3 Strong field regime

In order to highlight the effects of surface anchoring, it is necessary to break this anchoring by increasing the amplitude of applied electric field. This process speeds up the aging of

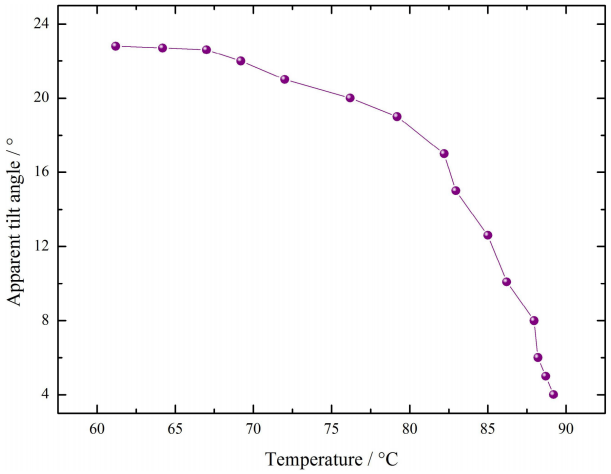

Fig. 6. The temperature dependence of tilt angle θ (C12F3 compound, 5 μm thick cell) follows Landau's first law perfectly.

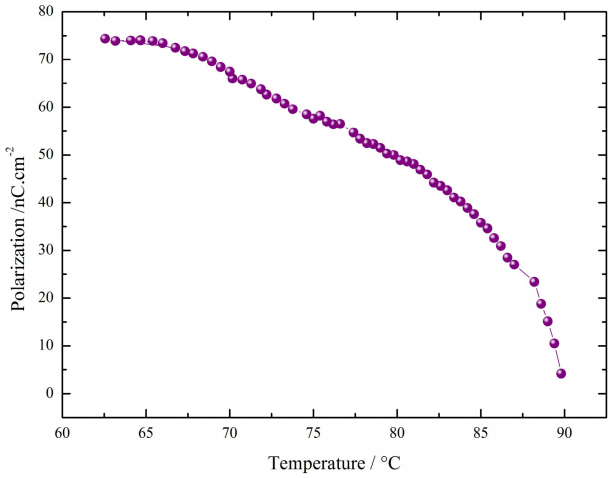

Fig. 7. Temperature dependence of spontaneous polarization (C12F3 compound, 5 μm thick cell).

the sample and can even destroy the cell. In this study, the same 3 μm thick cell was used as that for the dielectric measurements. The results are presented on the different diagrams of Fig. 8. A second peak P_2 clearly appears right after the first peak P_1 after excitation by a square or triangular voltage. Regarding P_2, two important considerations are reported:

- Its amplitude and surface are much smaller than that of the first peak (the surface represents about 3% of the first).
- It appears from a threshold field E_c.

All the experimental data presented below relates to a sample of the compound C12F3 confined in a planar anchoring cell with a thickness of 3 μm and for applied voltages between 10 and 30 Volts (Fig. 8).

The first peak results from a reversal of polarization in volume; it corresponds to the tilting of the molecules $+\theta \leftrightarrow -\theta$ with the applied electric field $+E \leftrightarrow -E$ (or vice versa). Molecules at the surfaces stay in the same inclined position and are only released when the modulus of the applied field is greater than the threshold value E_c. The reversal of polarization

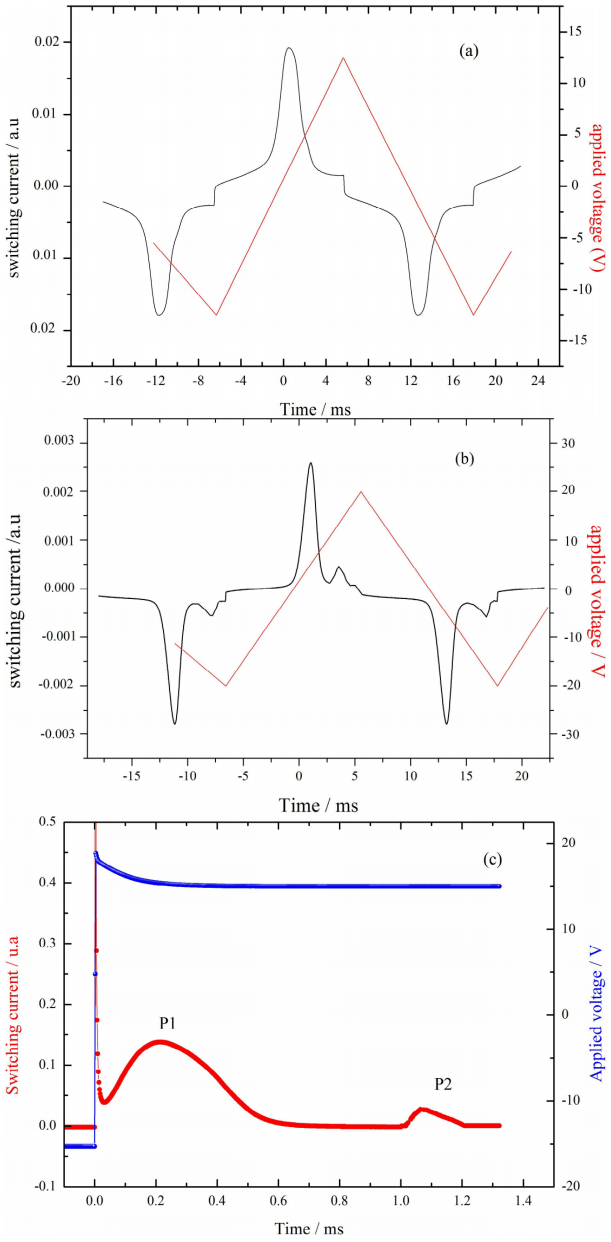

Fig. 8. A cell with product inside behaves like a capacitor. This cell is introduced into a simple circuit in parallel with a resistor R. A low frequency generator (40 Hz) powers the circuit and the voltage across the resistor is recorded. Two types of power supplies are considered: the first is a triangular voltage (a, b), while the second is a square one (c). The curves represent the responses of the system to different excitations at temperature T = 86.2 °C (SmC* Phase). (a, b) triangular excitation (red line), response (black line); 15 V–no second peak, 20 V–a second peak appears, and (c) 18 V–square excitation (blue line), a second peak appears as a response (red line).

at the surface creates a surplus of current, leading to a second peak P_2. The threshold field E_c gives the value of anchoring energy W_s, and the amplitude of the second peak gives information about the number of molecules involved.

We next proceed to the measurement of threshold voltages at which a second peak appears. The data are depicted in Fig. 9. Note that the variations in this threshold are similar to those

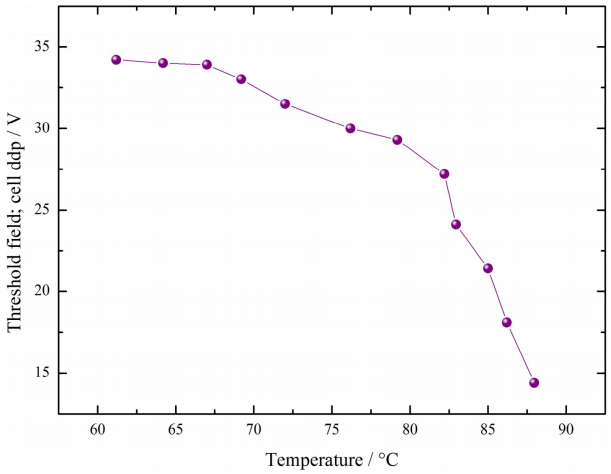

Fig. 9. Temperature dependence of the threshold field E_c (C12F3 compound, 5 μm thick cell).

in the tilt angle and polarization. These results further confirm the proportionality between the threshold field and the tilt angle.

3.4 Order of magnitude

From the measurements carried out on compound C12F3, the following values are obtained:

- The area of the first peak P_1 gives a polarization in the order of 30 nC/cm^2.
- The area of the second peak P_2 gives: $4\xi/d = 0.1$, that is, $\xi = 0.125$ μm with $d = 5$ μm.
- The coherence length ξ gives $K = PE\xi^2$ and $E = 4 \times 10^6$ V/m.

This gives $K = 1.87 \times 10^{-13}$ Newton.

The threshold field E_c gives $W_s = \sqrt{27KPE_c/2}$, that is, $W_s = 4 \times 10^{-5}$ J/m^2.

The value of the characteristic length λ_s can also be calculated from the relation $\lambda_s = k/W_s$, that is, $\lambda_s = 46$ A°. This value of λ_s corresponds to a fairly strong anchoring force.

4. Conclusions

The surface effects in chiral smectics have been studied extensively for several decades. The thermal shift and switching mechanism in electro-optical devices depend on cell thickness, surface conditions, tilt angle, and spontaneous polarization (Bawa et al., 1986). Several experimental studies have reported that surface anchoring and cell thickness also affect the transition temperature and magnitude of spontaneous polarization (Vaupotic and Copic, 2003; Bawa et al., 2020; Khan et al., 2021).

Through experimental observations in this work, it was possible to visualize the surface effects on the evolution of a chiral smectic liquid crystal sample confined in an SSFLC cell. The findings strongly support the established theoretical model to explain the observed transition shifts in these samples.

The calculations carried out in this study pave the way for the exploitation of experimental results in the determination of the characteristic parameters such as anchoring energy W_s and elastic constant K. These two quantities are fundamental for the understanding and control of ferroelectric liquid crystal devices.

In the proposed theoretical model, the volume part of free energy f contains only the curvature term in $\partial\varphi/\partial y$ and the ferroelectric coupling PE.

In future work, a more complete description of the energy could be achieved to improve the calculations by considering other elastic terms (spontaneous twist, splay deformation) as well as the flexoelectric and dielectric contributions of the system. Additionally, the dynamic aspect of this problem could potentially play a significant role in the model.

Conflict of interest

The authors declare no competing interest.

References

Bawa, A., Choudhary, A., Sharma, G., et al. Surface constraints controlled structural dynamics of ferroelectric liquid crystals. Applied Surface Science, 2020, 526 :146743.

Bawa, S. S., Biradar, A. M., Chandra, S. Frequency dependent polarization reversal and the response time of ferroelectric liquid crystal by triangular wave method. Japanese Journal of Applied Physics, 1986, 25: L446.

Biswas, S., Mukherjee, P. K. Confinement-driven smectic-A to chiral smectic-C∗ phase transition. Journal of Molecular Liquids, 2019, 287: 110913.

Cai, J., Sun, S., Wang, H. Current advances in capillarity: Theories and applications. Capillarity, 2023, 7(2): 25-31.

Chemingui, M., Soltani, T., Marcerou, J. P., et al. Effect of enantiomeric excess on the SmC* phase under electric field. Phase Transitions, 2016, 89(3): 221-231.

Clark, N. A., Lagerwall, S. T. Submicrosecond bistable electro-optic switching in liquid crystals. Applied Physics Letters, 1980, 36: 899-901.

Clark, N. A., Rieker, T. P. Erratum: Smectic-C "chevron," a planar liquid-crystal defect: Implications for the surface-stabilized ferroelectric liquid-crystal geometry. Physical Review A, 1989, 39: 5450.

Cole, K. S., Cole, R. H. Dispersion and absorption in dielectrics I. Alternating current characteristics. The Journal of Chemical Physics, 1941, 9: 341-351.

De Gennes, P. G., Prost, J. The Physic of Liquid Crystal, 2ed. Oxford, UK, Clarendon Press, 1993.

Dhaouadi, H., Zgueb, R., Riahi, O., et al. Field-induced phase transitions in chiral smectic liquid crystals studied by the constant current method. Chinese Physics B, 2016, 25(5): 057704.

Dupont, L., Galvan, J. M., Marcerou, J. P., et al. On the Smectic a Smectic C* phase transition in high polarization ferroelectric liquid crystals. Ferroelectrics, 1988, 84(1): 317-325.

Essid, S., Manai, M., Gharbi, A., et al. Synthesis and characterization of a novel liquid crystal series with tribenzoate

cores and monofluoro-substitution on the phenyl ring near the chiral chain. Liquid Crystals, 2004, 31: 1185-1193.

Guo, Q., Kexin, Y., Vladimir, C., et al. Ferroelectric liquid crystals: Physics and applications. Crystals, 2019, 9(9): 470.

Khan, S., Prakash, J., Chauhan, S., et al. Partially unwound helical mode in surface stabilized ferroelectric liquid crystal geometry. Journal of Molecular Liquids, 2020, 305: 112767.

Khan, S., Prakash, J., Chauhan, S. Weak anchoring resolved substrate interface and bulk mode processes in surface stabilized ferroelectric liquid crystal. Journal of Molecular Liquids, 2021, 325: 114705.

Kumar, S., Lokesh, K. G., Choudhary, A., et al. Ferroelectric ordering at interface of paraelectric phase of liquid crystal and solid substrate in confined geometry. Applied Surface Science, 2019, 496: 143695.

Lagerwall, S. T., Dahl, I. Ferroelectric liquid crystals. Molecular Crystals and Liquid Crystals, 1984, 114: 151-187.

Liu, M., Chen, Y., Cheng, W., et al. Controllable electromechanical stability of a torsional micromirror actuator with piezoelectric composite structure under capillary force. Capillarity, 2022, 5(3): 51-64.

Manai, M. Etude des propriétés électriques et optiques de cristaux liquides présentant des phases smectiques chirales et les phases frustrées SmQ et L. Bordeaux, Université Sciences et Technologies-Bordeaux I, 2006.

Patel, J. S., Goodby, J. W. The dependence of the magnitude of the spontaneous polarization on the cell thickness in ferroelectric liquid crystals. Chemical Physics Letters, 1987, 137: 91-95.

Riahi, O., Trabelsi, F., Dhaouadi, H., et al. Effect of defects and surface anchoring on the phase behavior of chiral smectic liquid crystals. Phase Transitions, 2017, 90(3): 299-311.

Roy, S. S., Majumder, T. P., Roy, S. K., et al. Effect of spontaneous polarization on smectic C^* smectic A^* phase transition temperature and the thickness dependence of the spontaneous polarization of ferroelectric liquid crystal. Liquid Crystals, 1998, 25(1): 59-62.

Sasaki, Y., Le, K. V., Aya, S., et al. High-resolution calorimetric study of phase transition in chiral smectic-C liquid crystalline phases. Physical Review E, 2012, 86: 061704.

Srivastava, A. K., Chigrinov, V. G., Kwok, H. S. Ferroelectric liquid crystals: Excellent tool for modern displays and photonics. Journal of the Society for Information Display, 2015, 23(6): 253-272.

Vaupotic, N., Copic, M. Effect of spontaneous polarization and polar surface anchoring on the director and layer structure in surface-stabilized ferroelectric liquid crystal cells. Physical Review E, 2003, 68: 061705.

Watson, S. J., Matkin, L. S., Baylis, L. J., et al. Influence of electric fields on the smectic layer structure of ferroelectric and antiferroelectric liquid crystal devices. Physical Review E, 2002, 65: 031705.

Yamada, K., Takanishi, Y. Sign inversion of liquid-crystal-induced circular dichroism observed in the Smectic-A and chiral smectic-C_α phases on binary mixture systems. Physical Review E, 1997, 56: R43-R46.

Zgueb, R., Dhaouadi, H., Othman, T. Dielectric relaxation spectroscopy and electro-optical studies of phase behaviour of a chiral smectic liquid crystal. Liquid Crystals, 2014, 14: 1394-1401.

Zgueb, R., Dhaouadi, H., Othman, T. Electro-optical properties and (E, T) phase diagram of fluorinated chiral smectic liquid crystals. Chinese Physics B, 2018, 27(10): 107701.

Appendix A. Euler-Lagrange equation: Limiting conditions

Consider a sample of liquid crystals with a volume V, surrounded by an area S. The total elastic energy of this sample is given by the following expression:

$$F = \iiint f_e(n_i, n_j)\, dV + \oiint f_s dS \tag{A1}$$

where f_e represents the volume energy density, n_i, n_j are the parameters that define the director $\vec{n}$, and f_s represents the surface energy density.

Take the case of a chiral smectic between two parallel planes at a distance d from one another, as shown in Fig. 1.

In this case, the director $\vec{n}$ is determined by the azimuth angle φ that makes its projection on the plane of the smectic layers (Oxy). The tilt angle θ is assumed to be constant. The Eq. (A1) can then be expressed in the following form:

$$F = \int_0^d f_e(\varphi, \dot{\varphi}) dy + f_{s1}(\varphi_1) + f_{s2}(\varphi_2) \tag{A2}$$

where $\dot{\varphi} = \partial\varphi/\partial y$.

Furthermore, F is a function of φ, which is preferably minimized.

Let:

$$\varphi(y) = \tilde{\varphi}(y) + \alpha w(y) \tag{A3}$$

where $w(y)$ is an arbitrary function of class C1, such that $F(\varphi) \geq F(\tilde{\varphi}), \alpha w(y)$ and α are an arbitrary constant.

Subsequently, Eq. (A2) becomes:

$$F = \int_0^d f_e(\tilde{\varphi} + \alpha w \dot{\varphi} + \alpha w) dy + f_{s1}(\varphi_1) + f_{s2}(\varphi_2) \tag{A4}$$

F must take a minimum value for $\alpha = 0 \Rightarrow (\partial F/\partial\alpha)_{\alpha=0} = 0$.

Then, we have:

$$df_e = \frac{\partial f_e}{\partial \varphi} d\varphi + \frac{\partial f_e}{\partial \dot{\varphi}} d\dot{\varphi} \tag{A5}$$

$$df_e = \frac{\partial f_e}{\partial \tilde{\varphi}} \frac{\partial \tilde{\varphi}}{\partial \varphi} \frac{\partial \varphi}{\partial \alpha} d\alpha + \frac{\partial f_e}{\partial \dot{\tilde{\varphi}}} \frac{\partial \dot{\tilde{\varphi}}}{\partial \dot{\varphi}} \frac{\partial \dot{\varphi}}{\partial \alpha} d\alpha \tag{A6}$$

From Eq. (A3), we can obtain:

$$\begin{cases} \dfrac{\partial \tilde{\varphi}}{\partial \varphi} = \dfrac{\partial \dot{\tilde{\varphi}}}{\partial \dot{\varphi}} = 1 \\ \dfrac{\partial \varphi}{\partial \alpha} = w \\ \dfrac{\partial \dot{\varphi}}{\partial \alpha} = \dot{w} \end{cases} \tag{A7}$$

$$df_e = \left(\frac{\partial f_e}{\partial \tilde{\varphi}} w + \frac{\partial f_e}{\partial \dot{\tilde{\varphi}}} \dot{w} \right) d\alpha \tag{A8}$$

On the other hand, we have:

$$\begin{cases} \dfrac{\partial f_{s1}}{\partial \alpha} = w(y=0) \dfrac{\partial f_{s1}}{\partial \tilde{\varphi}_1} \\ \dfrac{\partial f_{s2}}{\partial \alpha} = w(y=d) \dfrac{\partial f_{s2}}{\partial \tilde{\varphi}_2} \end{cases} \tag{A9}$$

As:

$$\frac{d}{dy}\left(\frac{\partial f_e}{\partial \dot{\tilde{\varphi}}} w \right) = \frac{d}{dy}\left(\frac{\partial f_e}{\partial \varphi} \right) w + \frac{\partial f_e}{\partial \dot{\tilde{\varphi}}} \dot{w} \tag{A10}$$

Then:

$$\frac{\partial f_e}{\partial \dot{\tilde{\varphi}}} \dot{w} = \frac{d}{dy}\left(\frac{\partial f_e}{\partial \dot{\tilde{\varphi}}} w \right) - \frac{d}{dy}\left(\frac{\partial f_e}{\partial \varphi} \right) w \tag{A11}$$

From Eqs. (A8)-(A10), we can deduce:

$$\frac{dH}{d\alpha} = \int_0^d \left[\frac{\partial f_e}{\partial \dot{\tilde{\varphi}}} \dot{w} + \frac{d}{dy}\left(\frac{\partial f_e}{\partial \dot{\tilde{\varphi}}} w \right) \right] dy + \frac{df_{s1}}{d\tilde{\varphi}_1} w_1 + \frac{df_{s2}}{d\tilde{\varphi}_2} w_2 \tag{A12}$$

$$\frac{dH}{d\alpha}=\int_0^d\left[\frac{\partial f_e}{\partial\tilde{\varphi}}-\frac{d}{dy}\left(\frac{\partial f_e}{\partial\dot{\tilde{\varphi}}}\right)\right]wdy+\left[-\left(\frac{\partial f_e}{\partial\dot{\tilde{\varphi}}}w\right)_{y=0}+\frac{df_{s1}}{d\tilde{\varphi}_1}w_1\right]+\left[\left(\frac{\partial f_e}{\partial\dot{\tilde{\varphi}}}w\right)_{y=d}+\frac{df_{s2}}{d\tilde{\varphi}_2}w_2\right] \tag{A13}$$

This quantity must be zero αw. Moreover, for $\alpha=0$, we have $\begin{cases}\tilde{\varphi}=\varphi\\ \dot{\tilde{\varphi}}=\dot{\varphi}\end{cases}$.

According to the Euler-Lagrange equation:

$$\frac{\partial f_e}{\partial\varphi}-\frac{d}{dy}\left(\frac{\partial f_e}{\frac{\partial\varphi}{\partial y}}\right)=0 \tag{A14}$$

where the limiting conditions are:

$$\begin{cases}\left[\frac{\partial f_e}{\partial\left(\frac{\partial\varphi}{\partial y}\right)}\right]_{y=d}=-\frac{df_{s2}}{d\varphi_2}\\ \left[\frac{\partial f_e}{\partial\left(\frac{\partial\varphi}{\partial y}\right)}\right]_{y=0}=\frac{df_{s1}}{d\varphi_1}\end{cases} \tag{A15}$$